

# Graphene-Based Infrared Lens with Tunable Focal Length

Yan Xiu Li, Fan Min Kong<sup>\*</sup>, and Kang Li

**Abstract**—In modern information and communication technologies, manipulating focal length has been hot topic. Considering that the conductivity of graphene layer can effectively be tuned by purposely designing the thickness of the dielectric spacer underneath the graphene layer, a graphene-based lens with tunable focal length is proposed in this paper, and it can be used to collimate waves. The fabrication of the proposed graphene-based lens is purposed, and the performance of the lens is verified with finite-element method. The simulation results demonstrate that the graphene-based lens has excellent tunability and confinement. At the same time, the lens exhibits low loss in certain rang and large frequency bandwidth.

## 1. INTRODUCTION

Emerging within the last decades, because of the ability to overcome the diffraction limit of light in microchip-sized devices, surface plasmon polaritons (SPPs) have attracted great and renewed interest [1–3]. Subsequently, it has aroused great interest in exploring various plasmonic devices [4–10]. In previous works, plasmonic devices are generally made of conventional noble metals. However, most plasmonic devices based on conventional noble metals, such as silver and gold, have enormous loss and cannot be tuned [11, 12], hence limit the propagation length of SPP wave and the tunability of the metallic plasmonic devices.

Since monolayer graphene was found, it has attracted special attention in optical field [13–15]. Compared with conventional noble metals, graphene possesses unprecedented advantages, including flexible tunability [12, 16, 17], extremely tight confinement [18], and low losses at THz and mid-infrared region [19, 20]. With these striking electrical and optical properties, graphene has been regarded as a novel plasmonic material.

The effective mode index for the SPP wave along the graphene layer can reach 100, with effective wavelength much smaller than that in free space. As a result, the plasmon polariton wave can be tightly confined to the graphene layer, and the damping loss of the plasmon polariton is relatively low. With these advantages, graphene has been proved to be a suitable alternative material to conventional noble metals.

The ability to manipulate the focal length is at the heart of modern information and communication technologies. In recent years, many plasmonic devices based on noble metals have been proposed theoretically and demonstrated experimentally [21–23]. It is proved that the propagation of SPP wave can be flexibly controlled by carefully tuning the dielectric material properties adjacent to a metal through transformation optics method. Different from the above metal-based plasmonic devices, a graphene-based lens with tunable focal length by designing the thickness of dielectric spacer beneath the graphene layer is proposed in this paper. In addition, the dispersion of the proposed lens is investigated. Finally, the simulation results with different frequencies are presented to demonstrate the broadband design concept. The method of designing the graphene lens in this paper will pave the way to effectively change the focal length of lens at nanoscale.

---

*Received 2 December 2015, Accepted 10 January 2016, Scheduled 13 January 2016*

<sup>\*</sup> Corresponding author: Fan Min Kong (kongfm@sdu.edu.cn).

The authors are with the School of Information Science and Engineering, Shandong University, Jinan 250100, China.

## 2. THEORETICAL ANALYSIS

The complex conductivity ( $\sigma_g = \sigma_{g,r} + i\sigma_{g,i}$ ) of graphene is determined by Kubo formula [24]:

$$\sigma(\omega, \mu_c, \Gamma, T) = -\frac{ie^2(\omega + i2\Gamma)}{\pi\hbar^2} \left[ \frac{1}{(\omega + i2\Gamma)^2} \times \int_0^\infty \xi \left( \frac{\partial f_d(\xi)}{\partial \xi} - \frac{\partial f_d(-\xi)}{\partial \xi} \right) d\xi - \int_0^\infty \frac{f_d(-\xi) - f_d(\xi)}{(\omega + i2\Gamma)^2 - 4(\xi/\hbar)^2} d\xi \right], \quad (1)$$

where  $\omega$  is the radian frequency,  $\mu_c$  the chemical potential,  $\Gamma$  the phenomenological scattering rate,  $T$  the temperature,  $f_d(\xi) = (e^{(\xi - \mu_c)/k_B T} + 1)^{-1}$  the Fermi-Dirac distribution,  $e$  the electron charge,  $\hbar = h/2\pi$  the reduced Planck's constant,  $\xi$  the energy, and  $k_B$  the Boltzmann's constant [25, 26].

The imaginary part of graphene conductivity can be negative or positive values in different ranges of frequency via external tunability. When  $\sigma_{g,i} > 0$ , a graphene layer is capable of supporting a transverse-magnetic (TM) SPP wave, which behaves as a very thin metal layer, and when  $\sigma_{g,i} < 0$ , a weak transverse-electric (TE) SPP wave might be present [24, 27, 28].

Here, it is considered that a graphene layer is located between two different dielectrics characterized by relative permittivities  $\varepsilon_0$  and  $\varepsilon_d$ , respectively. According to Dyadic Green's function, the dispersion relation of TM SPP surface wave can be expressed as [29]:

$$\frac{\varepsilon_0}{\sqrt{k_p^2 - \varepsilon_0\omega^2/c^2}} + \frac{\varepsilon_d}{\sqrt{k_p^2 - \varepsilon_d\omega^2/c^2}} = -\frac{i\sigma_g}{\omega\varepsilon_0}, \quad (2)$$

where  $k_p$  is the wave number of the guided TM SPP wave and  $k_0$  the wave number of excitation light in free space expressed as  $\omega/c$ . For an isolated graphene layer, there is  $\varepsilon_0 = \varepsilon_d = 1$ . Eq. (2) can be simplified as [24, 27]:

$$k_p = k_0 \sqrt{1 - (2/\eta_0\sigma_g)^2}, \quad (3)$$

where  $\eta_0 \approx 377 \Omega$  denotes the intrinsic impedance of free space.

For an isolate graphene sheet, the chemical potential is determined by the carrier density [24]:

$$n_s = \frac{2}{\pi\hbar^2 V_f^2} \int_0^\infty \xi [f_d(\xi) - f_d(\xi + 2\mu_c)] d\xi, \quad (4)$$

here  $V_f$  is the Fermi velocity and  $n_s$  the sheet doping of graphene. In the analysis,  $\mu_c = \hbar V_f \sqrt{\pi n_s}$  and  $V_f = 10^6$  m/s [30].

The most important advantage of graphene is the tunability of conductivity. The carrier density can be tuned by changing the thickness of the dielectric spacer underneath the graphene layer, which influences the dispersion and intraband losses of graphene. Therefore, surface carrier density  $n_s$  can also be depicted as [13]:

$$n_s = \varepsilon_0 \varepsilon_d V_g / h e, \quad (5)$$

where  $h$  is the thickness of the spacer and  $V_g$  the gate voltage. Thus, according to Eqs. (4) and (5), the relationship between the thickness of the spacer and the focal length can be obtained.

## 3. DESIGN A GRAPHENE-BASED LENS WITH TUNABLE FOCAL LENGTH

The graphene-based lens can be fabricated into circular symmetry, and it is a type of aberration-free lens. The lens focus can be changed inside the circle, and it has high efficiency and accuracy in controlling the focal length. The corresponding new refractive index profile of the graphene-based lens is given as [31]:

$$n(r) = n_0 / d(R^2 + d^2 - r^2)^{1/2}, \quad (6)$$

where  $r$  is the distance away from the center of the lens,  $d$  the focal length,  $R$  the radius of the designed graphene lens, and  $n_0$  the refractive index of the background graphene on which the lens is designed. It is pertinent that the index of refraction in the designed lens is  $n_0$  at  $r = R$ , and the lens is, therefore,

matched to the surrounding circumstances. The relationships between the refractive index and the parameter  $r$  are presented in Fig. 1, when  $d$  is set at different values.

According to Eq. (1), when the working frequency is set at  $f = 50$  THz, temperature is  $T = 300$  K, and the phenomenological scattering rate is  $\Gamma = 0.43$  meV. The relationship curve between graphene's complex conductivity and chemical potential is given in Fig. 2.

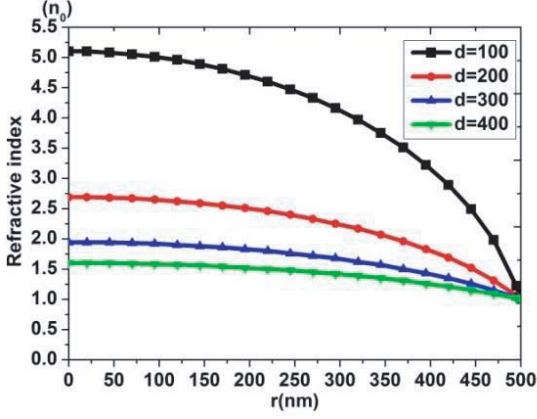


**Figure 1.** Lateral profile of the refractive index with  $d = 100, 200, 300,$  and  $400$  nm.

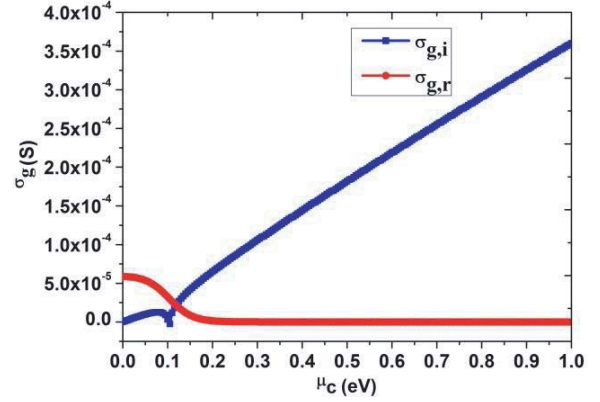


**Figure 2.** The relationship curves between graphene's complex conductivity and chemical potential at  $f = 50$  THz,  $T = 300$  K, and  $\Gamma = 0.43$  meV.

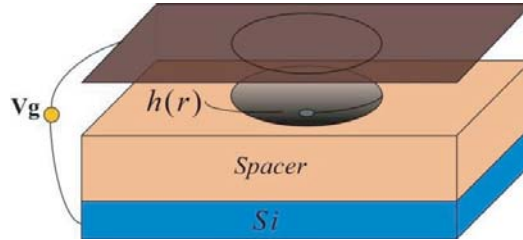


**Figure 3.** Schematic diagram of the designed graphene lens,  $h$  represents the thickness of dielectric spacer.

From Fig. 2, it can be found that when the chemical potential is in the range  $\mu_c > 0.175$  eV, the real part of conductivity is nearly zero (i.e., the loss of graphene is nearly zero). However, when the chemical potential is out of that range, the real part of conductivity is very large, which implies that the device is lossy. When the real part is much smaller than its imaginary part, the dispersion relationship can be approximately written as [32]:

$$n_{spp} = \frac{k_p}{k_0} \approx \frac{2}{\sigma_{g,i}\eta_0}, \tag{7}$$

where  $\sigma_{g,i}$  is the imaginary part of graphene conductivity.

To analog the same spatial variation, the effective mode index of the SPP wave should vary spatially according to Eq. (6):

$$n_{spp} = n(r), \tag{8}$$

From Eq. (6), it can be known that the lens designed in this paper is a graded-index lens, and the thickness of the spacer is a function of the radial coordinate. The gradual variation of the refractive index can be modeled as a gradual variation of the graphene conductivity by changing the thickness of the spacer. With Eqs. (5) (7) and (8), the relationship of the thickness of the spacer  $h$  and  $r$  can be obtained, if  $d$  is fixed.

The schematic diagram of the proposed lens is shown in Fig. 3. The graphene-based lens consists of a graphene layer with chemical potential  $\mu_c$ , which is separated from a silicon (Si) substrate by a dielectric spacer. It can be seen that the thickness of the spacer  $h$  changes gradually from the center to periphery along the  $r$  direction. It is assumed that the surrounding medium is air, and the SPP wave is excited in right.

#### 4. SIMULATION RESULTS AND DISCUSSIONS

In the following simulations, the parameters are set as follows:  $f = 50$  THz,  $\Gamma = 0.43$  meV and  $T = 300$  K. Under the above conditions, the conductivity of graphene depends on its chemical potential from Eq. (1). Generally, the energy dissipation of a system can be evaluated by the real part of the material's conductivity. From Fig. 2, it can be seen that when the chemical potential is low, such as less than 0.175 eV, the real part of the graphene conductivity is very large, and the loss is very large. Consequently, the surface of graphene cannot support the propagation of SPP.

In this paper,  $V_g$  is 30 V,  $R$  500 nm,  $\varepsilon_d$  3.9, and  $n_0$  14.9 which is chosen because chemical potential is larger than 0.175 eV, in which range the device is dispersionless. The characteristics of the SPP wave propagating along the graphene surface are controlled by elaborately adjusting the thickness of the dielectric spacer underneath the graphene layer, which will produce an inhomogeneous chemical potential distribution and induce a nonuniform conductivity pattern along the graphene layer. According to above analysis, relationships of  $r$  and the imaginary part of graphene conductivity are presented in Fig. 4(a) and the relationships of  $r$  and the thickness of the spacer presented in Fig. 4(b). The design process is realized by electron beam lithography and etching method [33, 34].

To demonstrate the performance of the lens, the finite element method is used. Fig. 5(a) demonstrates the  $z$  components of electric field of the TM SPP wave with the focal lengths 100, 200, 300, and 400 nm at  $f = 50$  THz. For simplicity, it is assumed that a free-standing graphene layer is applied in free space with the spatially inhomogeneous conductivity patterns. The simulation results show that when a SPP plane wave excited from right propagates along the graphene layer, it can be transformed to a point source. The experimentally obtained electric field maps with the proposed lens are shown in Fig. 5(a).

When the SPP plane wave propagates along the graphene from the right and converges into a point, the electric field norm will change. As a result, the performance of the proposed lens can be estimated by measuring the electric field norm at the focal line. As shown in Fig. 6(b), the electric field norm profiles of incident wave with  $|E_0| = 1$  V/m are compared across the graphene sheet with the focal lengths of 100, 200, 300, and 400 nm. From Fig. 6(b), it can be seen that when  $d = 100$  nm, the imaginary part of the graphene conductivity is small, and the ratio of the imagine part to its real part

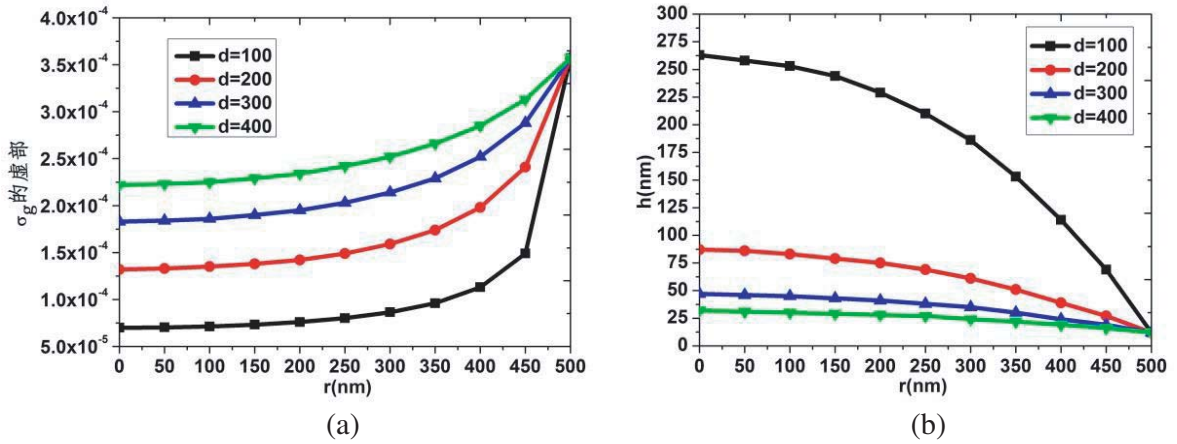


**Figure 4.** (a) The conductivity distribution of the graphene sheet, (b) the thickness profile of the dielectric spacer, with the focal lengths of 100, 200, 300, and 400 nm.

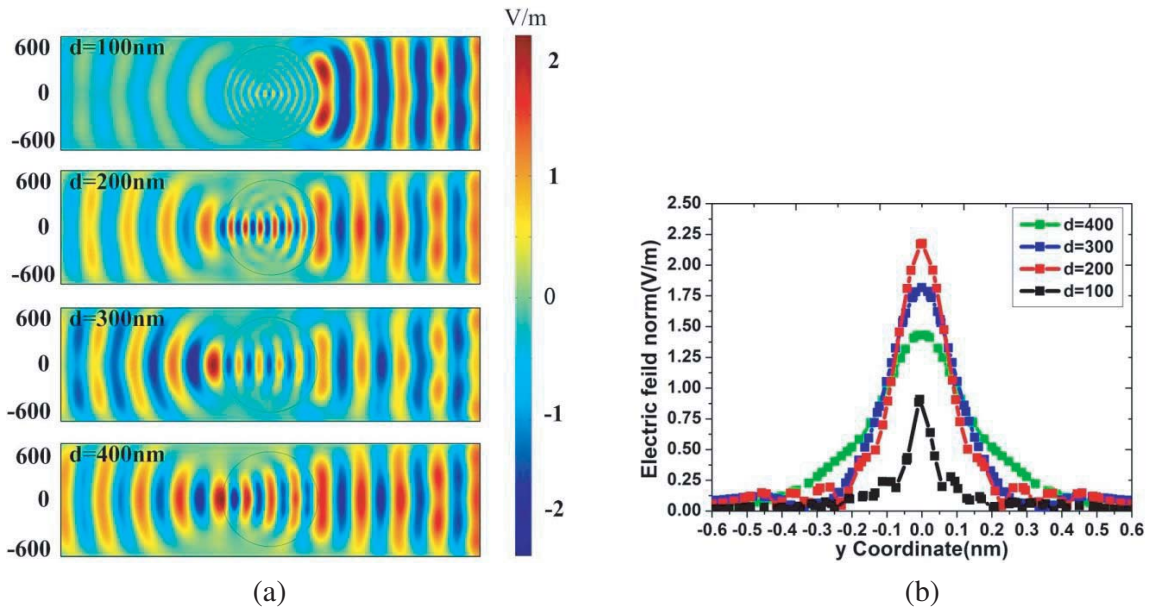


**Figure 5.** (a) The profiles of the electric field  $E_z$ , (b) comparison of electric field norm, of a SPP wave propagating along the graphene layer with  $d = 100, 200, 300,$  and  $400$  nm at  $f = 50$  THz.

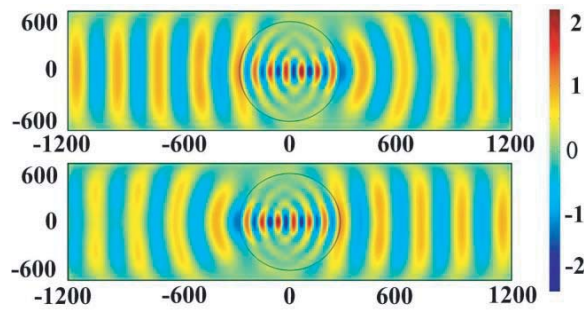


**Figure 6.** The electric field distribution maps with the electric dipole located in  $200$  nm (above) and  $-200$  nm (below).

is not large enough. The real part cannot be ignored; therefore, the energy is heavily dissipated across the propagating direction, and the electric field norm is less than  $|E_0|$ , while they are much larger than  $|E_0|$  with  $d = 200, 300,$  and  $400$  nm. While the imaginary part of graphene conductivity is large relative to its real part, the real part can be ignored, and the incident wave can converge into the focal area with relative low dissipation losses. In addition, the proposed lens has better performance with  $d = 200$  nm than that with  $d = 100, 300,$  and  $400$  nm.

The graphene-based lens can also be used to be a planar collimating lens. As we all know, an electric dipole can excite a SPP spherical wave. When an electric dipole is set at any point within the graphene-based lens, a SPP plane wave will be present in the opposite side. The electric field distribution maps are presented in Fig. 6, when the electric dipole is located in  $200$  nm and  $-200$  nm along the lateral axis.

To confirm the bandwidth, electric field data are acquired over a number of the frequencies. Electric field profiles are shown in Fig. 7, corresponding to the frequencies  $42$  THz,  $46$  THz,  $54$  THz and  $58$  THz with  $d = 200$  nm. Due to the refractive index distribution remains unchanged for different incident frequencies, and the proposed lens can always focus light at the same position by varying the dielectric spacer thickness  $h$ . In all cases, the beam is converged into a point area.

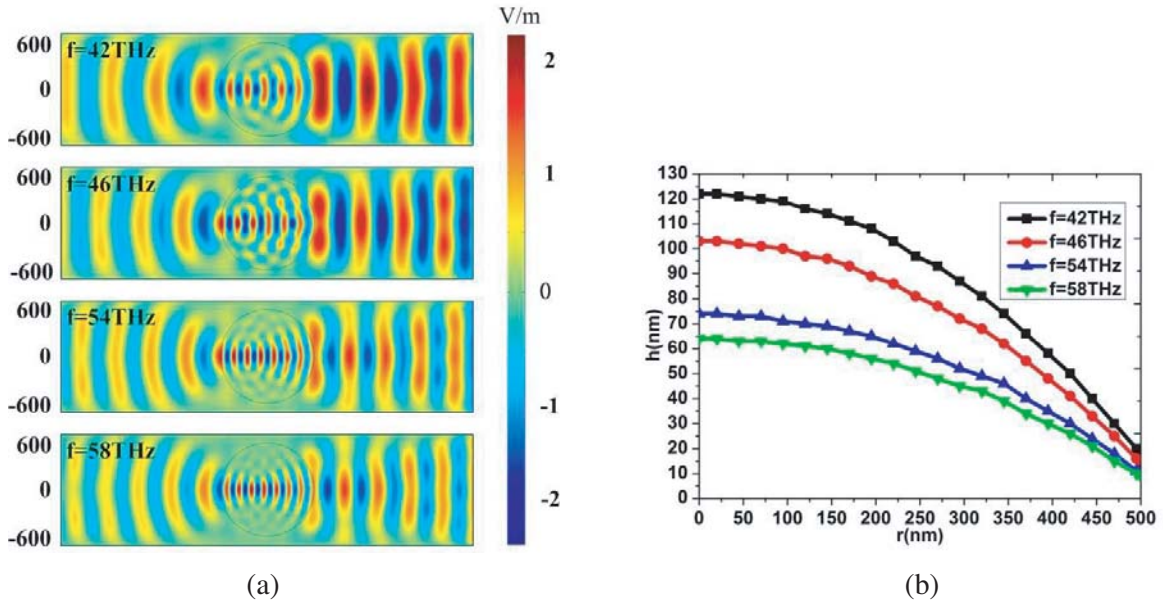


**Figure 7.** (a) The profiles of the electric field  $E_z$  of a SPP wave propagating along the graphene layer, (b) the thickness profile of the dielectric spacer, with  $d = 200$  nm at  $f = 42, 46, 54,$  and  $58$  THz.

## 5. SUMMARY

In conclusion, a graded index graphene-based lens with tunable focal length is proposed and investigated. The graphene conductivity can be easily tuned by changing the dielectric spacer thickness. Based on this principle, the graphene-based lens is purposely designed, and finite element simulations are performed to characterize the optical properties of the lens designed in this paper. It is found that the proposed method is practicable to design graphene-based lens with tunable focal length at different frequencies. It is also demonstrated that the proposed lens is dispersionless in a certain range. As an important application of the graphene-based lens, the field distributions are performed for different focal lengths. In addition, the lens can be used to collimate waves, and it possesses ultra-compact dimension and flexible tunability. This platform will help to shrink the size of an integrated photonic component and accelerate the speed of optical signal processing in the future.

## ACKNOWLEDGMENT

This work was supported by the National Natural Science Foundation of China (Nos. 61475084 and 61327808) and the Fundamental Research Funds of Shandong University (No. 2014JC032).

## REFERENCES

1. Bozhevolnyi, S. I., V. S. Volkov, E. Devaux, J.-Y. Laluet, and T. W. Ebbesen, "Channel plasmon subwavelength waveguide components including interferometers and ring resonators," *Nature*, Vol. 440, 508–511, 2006.
2. Engheta, N., "Circuits with light at nanoscales: Optical nanocircuits inspired by metamaterial," *Science*, Vol. 317, 1698–1702, 2007.
3. Ebbesen, T. W., C. Genet, and S. I. Bozhevolnyi, "Surface-plasmon circuitry," *Physics Today*, Vol. 61, 44, 2008.
4. De Leon, I. and P. Berini, "Amplification of long-range surface plasmons by a dipolar gain medium," *Nature Photonics*, Vol. 4, 382–387, 2010.

5. He, S., Y. He, and Y. Jin, "Revealing the truth about 'trapped rainbow' storage of light in metamaterial," *Scientific Reports*, Vol. 2, 2012.
6. Gan, Q., Y. J. Ding, and F. J. Bartoli, "Rainbow trapping and releasing at telecommunication wavelengths," *Physical Review Letters*, Vol. 102, 056801, 2009
7. Hu, H., D. Ji, X. Zeng, K. Liu, and Q. Gan, "Rainbow trapping in hyperbolic metamaterial waveguide," *Scientific Reports*, Vol. 3, 2013.
8. Wang, G., H. Lu, and X. Liu, "Trapping of surface plasmon waves in graded grating waveguide system," *Applied Physics Letters*, Vol. 101, 013111, 2012.
9. Politano, A. and G. Chiarello, "Quenching of plasmons modes in air-exposed graphene-Ru contacts for plasmonic devices," *Applied Physics Letters*, Vol. 102, 201608, 2013.
10. Politano, A. and G. Chiarello, "Unravelling suitable graphene-metal contacts for graphene-based plasmonic devices," *Nanoscale*, Vol. 5, 8215–8220, 2013.
11. Koppens, F. H., D. E. Chang, and F. J. Garcia de Abajo, "Graphene plasmonics: A platform for strong light–matter interactions," *Nano Letters*, Vol. 11, 3370–3377, 2011.
12. Fang, Z., S. Thongrattanasiri, A. Schlather, Z. Liu, L. Ma, Y. Wang, et al., "Gated tunability and hybridization of localized plasmons in nanostructured graphene," *ACS Nano*, Vol. 7, 2388–2395, 2013.
13. Novoselov, K. S., A. K. Geim, S. Morozov, D. Jiang, Y. Zhang, S. A. Dubonos, et al., "Electric field effect in atomically thin carbon films," *Science*, Vol. 306, 666–669, 2004.
14. Grigorenko, A., M. Polini, and K. Novoselov, "Graphene plasmonics," *Nature Photonics*, Vol. 6, 749–758, 2012.
15. Bonaccorso, F., Z. Sun, T. Hasan, and A. Ferrari, "Graphene photonics and optoelectronics," *Nature Photonics*, Vol. 4, 611–622, 2010.
16. Politano, A. and G. Chiarello, "Probing Young's modulus and Poisson's ratio in graphene/metal interfaces and graphite: A comparative study," *Nano Research*, 1–10, 2014.
17. Matis, B. R., J. S. Burgess, F. A. Bulat, A. L. Friedman, B. H. Houston, and J. W. Baldwin, "Surface doping and band gap tunability in hydrogenated graphene," *ACS Nano*, Vol. 6, 17–22, 2012.
18. Politano, A., D. Campi, V. Formoso, and G. Chiarello, "Evidence of confinement of the  $\pi$  plasmon in periodically rippled graphene on Ru(0001)," *Physical Chemistry Chemical Physics*, Vol. 15, 11356–11361, 2013.
19. Politano, A. and G. Chiarello, "Plasmon modes in graphene: Status and prospect," *Nanoscale*, Vol. 6, 10927–10940, 2014.
20. Rast, L., T. Sullivan, and V. Tewary, "Stratified graphene/noble metal systems for low-loss plasmonics applications," *Physical Review B*, Vol. 87, 045428, 2013.
21. Liu, Y., T. Zentgraf, G. Bartal, and X. Zhang, "Transformational plasmon optics," *Nano Letters*, Vol. 10, 1991–1997, 2010.
22. Zentgraf, T., Y. Liu, M. H. Mikkelsen, J. Valentine, and X. Zhang, "Plasmonic luneburg and eaton lenses," *Nature Nanotechnology*, Vol. 6, 151–155, 2011.
23. Della Valle, G. and S. Longhi, "Graded index surface-plasmon-polariton devices for subwavelength light management," *Physical Review B*, Vol. 82, 153411, 2010.
24. Hanson, G. W., "Dyadic Green's functions and guided surface waves for a surface conductivity model of graphene," *Journal of Applied Physics*, Vol. 103, 064302, 2008.
25. Wang, W., S. P. Apell, and J. M. Kinaret, "Edge magnetoplasmons and the optical excitations in graphene disks," *Physical Review B*, Vol. 86, 125450, 2012.
26. Fallahi, A. and J. Perruisseau-Carrier, "Design of tunable biperiodic graphene metasurfaces," *Physical Review B*, Vol. 86, 195408, 2012.
27. Vakil, A. and N. Engheta, "Transformation optics using graphene," *Science*, Vol. 332, 1291–1294, 2011.
28. Mikhailov, S. and K. Ziegler, "New electromagnetic mode in graphene," *Physical Review Letters*, Vol. 99, 016803, 2007.

29. Zeng, C., X. Liu, and G. Wang, “Electrically tunable graphene plasmonic quasicrystal metasurfaces for transformation optics,” *Scientific Reports*, Vol. 4, 2014.
30. Gao, W., J. Shu, C. Qiu, and Q. Xu, “Excitation of plasmonic waves in graphene by guided-mode resonances,” *ACS Nano*, Vol. 6, 7806–7813, 2012.
31. Gutman, A., “Modified luneberg lens,” *Journal of Applied Physics*, Vol. 25, 855–859, 1954.
32. Xu, H. J., W. B. Lu, Y. Jiang, and Z. G. Dong, “Beam-scanning planar lens based on graphene,” *Applied Physics Letters*, Vol. 100, 051903, 2012.
33. Bolotin, K., K. Sikes, J. Hone, H. Stormer, and P. Kim, “Temperature-dependent transport in suspended graphene,” *Physical Review Letters*, Vol. 101, 096802, 2008.
34. Dorgan, V. E., A. Behnam, H. J. Conley, K. I. Bolotin, and E. Pop, “High-field electrical and thermal transport in suspended graphene,” *Nano Letters*, Vol. 13, 4581–4586, 2013.